Journal of Sound and Vibration (2001) **248**(4), 653–669
doi:10.1006/jsvi.2001.3809, available online at http://www.idealibrary.com on IDEAL®

SOME DISCONTINUOUS BIFURCATIONS IN A TWO-BLOCK STICK–SLIP SYSTEM

U. GALVANETTO

Department of Aeronautics, Imperial College of Science, Technology and Medicine, Prince Consort Road, London SW7 2BY, England. E-mail: u.galvanetto@ic.ac.uk

(*Received* 12 *December* 2000, *and in final form* 3 *May* 2001)

Non-smooth dynamical systems exhibit continuous and discontinuous bifurcations. Continuous bifurcations are well understood and described in many textbooks, whereas discontinuous bifurcations are still the object of active research. Grazing bifurcations, C-bifurcations and other types of bifurcations characterized by jumps of the relevant Floquet multipliers have been described in the scientific literature. This paper deals with two discontinuous bifurcations found in mechanical systems affected by dry friction.
© 2001 Academic Press

1. INTRODUCTION

When modelling natural dynamical phenomena a good first mathematical approach is to consider a smoothly varying system. However, there are many examples of physical systems where a smooth approximation breaks down since the system undergoes a series of sudden, rapid changes in state. The mechanical sciences offer several examples of this type of systems.

- The transversal oscillations of railway bogies occur smoothly up to the point where the flange of the wheel hits the railway track; at this stage a new dynamics begins which terminates when the flange is no longer in contact with the track [1].
- In a similar way the oscillations of suspension bridges may be influenced by variable stiffness with very fast variations since the suspension cables are much stiffer in tension than in compression [2].
- The dynamics of systems idealized by a block with non-smooth surface excited on a flat plate is hugely influenced by the properties of the transition between different portions of the contact surface [3].
- The free motion of a mechanical system may be changed abruptly by an impact, which usually strongly affects the velocity of the system. The motion can then evolve freely until the next impact and so on [4–6].
- In systems affected by dry friction slip or stick, phases are separated by sudden stick–slip or slip–stick transitions. In the simplest descriptions of frictional phenomena, during the stick phase there is zero relative velocity between the surfaces in contact whereas the velocity is different from zero during a slip phase. Therefore, the dimension of the phase space of a dynamic system with dry friction forces may change with time [7–12].

All previous examples are taken from mechanical sciences and structural engineering, which are the fields of major expertise of the author. However, similar systems can also be found in many different areas of science such as electronics [13], biology (integrate and fire

0022-460X/01/490653 + 17 $35.00/0 © 2001 Academic Press

concepts in biology, such as heart beats), economics (sudden drops in stock market shares, etc.), etc.

The above-mentioned phenomena are usually represented as piecewise smooth (PWS) systems. Depending upon the application, the mathematical model may vary but there are many common features. To explain some of the issues consider a system with n degrees of freedom represented by the vector $x \in \mathbb{R}^n$. In $\mathbb{R}^n$ there exists (at least) a discontinuity surface S which is intersected by the trajectory of the system at $t = t_1$. The dynamics of the system is described by two sets of differential equations, f_1 for $t < t_1$ and f_2 for $t > t_1$

$$t < t_1, \quad x(t_0) = x_0, \quad \dot{x} = f_1(x), \quad f_1(x) \in C^1, \tag{1}$$

$$t = t_1, \quad S(x(t_1)) = 0, \quad x(t_{1+}) = g(x(t_{1-})), \quad S \in C^1, \tag{2}$$

$$t > t_1, \quad x(t_1) = x(t_{1+}), \quad \dot{x} = f_2(x), \quad f_2(x) \in C^1. \tag{3}$$

In an impacting system f_1 and f_2 usually have the same expression but the transition condition (2) defines how the velocities vary after an impact, which usually causes a discontinuity at least in the component of the velocity normal to the impact surface. The discontinuity surface S for impacting systems is usually expressed as a function of the displacement components of the system, whereas in stick–slip systems the expression of $S(x) = 0$ also involves some velocity components. In a stick–slip system there is no discontinuity in the phase variable values when S is crossed but there is a discontinuity in the accelerations and a change in the number of equations describing the dynamics of the system. Therefore, f_1 and f_2 are function vectors with different number of components because the number of unknown velocities in a slip phase is different from the number of unknown velocities during a preceding or following stick phase [7–9]. In railway dynamics or in suspension bridges the stiffness term in f_1 is different from the same term in f_2 and similar differences apply in the case of rolling blocks.

Different classifications are adopted for non-smooth systems: sometimes [14] systems with no discontinuity in the phase variables are called the Filippov systems [15]. Stick–slip problems and variable stiffness systems are of Filippov's type, whereas impacting systems are not, since their velocities may be discontinuous. From another point of view the impacting and variable stiffness systems may be classified as belonging to the same category (systems with constant dimension of the phase space), whereas stick–slip models are characterized by a variable dimension of the phase space.

The rest of the paper is organized as follows: section 2 briefly resumes basic concepts regarding discontinuous bifurcations. Section 3 describes the stick–slip model and defines the one-dimensional event map that is then used in section 4 to investigate the discontinuous bifurcations of the mechanical system.

2. DISCONTINUOUS BIFURCATIONS IN NON-SMOOTH SYSTEMS

Consider a continuous-time dynamic system:

$$\dot{x} = f(x, \mu) \quad x \in \mathbb{R}^n, \mu \in \mathbb{R}. \tag{4}$$

As the parameter μ changes, the limit sets of the system also change and typically a small change in μ produces small quantitative changes in a limit set. There is also the possibility that a small change in μ can cause a limit set to undergo a qualitative change. Loosely speaking such a qualitative change is called a bifurcation and the value of μ at which

a bifurcation occurs is called a bifurcation value. In the present work, the definition given in reference [14] is adopted: a value μ^* of the parameter is a bifurcation value if the number of periodic solutions changes for $\mu = \mu^*$ and the set (x^*, μ^*) is called a bifurcation point. A bifurcation point is a discontinuous bifurcation point if the Floquet multipliers of the periodic solution x^* are set valued and contain a value on the unit circle.

In recent decades many textbooks about bifurcation theory of smooth systems appeared and bifurcation of fixed points or periodic solutions in smooth vector fields are well understood [14, 16]. Bifurcations of non-smooth vector fields are currently the focus of active research, but there is still a lack not only in a systematic classification of them but also in a complete description of the variety of different bifurcations that affect non-smooth systems. Standard fold and flip bifurcations have been found and described in some non-smooth systems. Often the easiest way to visualize them is to define a one-dimensional map of a suitable variable of the system [9, 17]. In some other cases some smoothing procedures were introduced to simulate approximately the behaviour of non-smooth systems [12].

A smaller, but rapidly increasing, number of publications seems to describe non-conventional bifurcations in non-smooth systems. Nordmark [18] has introduced the concept of grazing bifurcation, which was then studied by several authors, especially in the field of impacting systems, but also in the area of stick–slip systems [19]. In the field of Filippov systems, di Bernardo, Feigin *et al.* [20] have defined "C-bifurcations" which are classified according to the number of real-valued eigenvalues of the Poincaré map.

Non-conventional bifurcations of non-smooth discrete mappings were also addressed by Nusse and Yorke [21] and Banerjee *et al.* [22].

The present paper describes, using a pragmatic engineering approach, two discontinuous bifurcations of periodic orbits, affecting continuous-time stick–slip mechanical systems.

3. THE MECHANICAL MODEL

The non-smooth system to be investigated, shown in Figure 1, is composed of two blocks on a moving belt. The velocity of the belt is constant and is called the driving velocity v_{dr}. Each block is connected to a fixed support and to the other block by elastic springs as shown in the figure. The surface between the blocks and the belt is rough so that the belt exerts a dry friction force on each block that sticks on the belt to the point where the elastic forces due to the springs exceed the maximum static friction force. At this point the block starts slipping and the slipping motion will continue to the point were the velocity of the block will be equal to that of the belt and the elastic forces will be equilibrated by the static friction force. The continuous repetition of this type of motions generates a stick–slip oscillation.

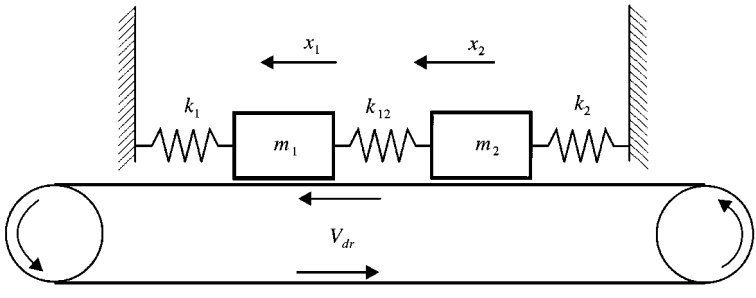

Figure 1. Stick–slip model under investigation.

During a stick phase the displacement of a block is given as a function of time:

$$x_i(t) = x_i(t_0) + v_{dr}(t - t_0), \quad i = 1, 2, \tag{5}$$

where x_i is the displacement of the generic block from a reference configuration in which all springs assume their natural length, and $x_i(t_0)$ is the initial displacement. The blocks can stick on the belt only if the following relations are true:

$$\begin{aligned} -f_{s1} < k_1 x_1 + k_{12}(x_1 - x_2) < f_{s1}, \\ -f_{s2} < k_2 x_2 + k_{12}(x_2 - x_1) < f_{s2}, \end{aligned} \tag{6}$$

where f_{si} is the maximum static friction force acting on block i, k_i is the stiffness of the spring connecting block i to the fixed support and k_{12} is the stiffness of the coupling spring as shown in Figure 1. Since the motion of the belt is in the direction of positive block displacements the stick phase will end on the right extremes of the intervals (6), i.e., where $k_1 x_1 + k_{12}(x_1 - x_2) = f_{s1}$ or $k_2 x_2 + k_{12}(x_2 - x_1) = f_{s2}$. If the first condition is verified then block 1 will start slipping, whereas the second condition indicates the impending slip condition for block 2. At one of these points a slip phase will begin according to the following equations of motion:

$$\begin{aligned} m_1 a_1(t) + k_1 x_1(t) + k_{12}(x_1(t) - x_2(t)) = f_{k1}(\dot{x}_1 - v_{dr}), \\ m_2 a_2(t) + k_2 x_2(t) + k_{12}(x_2(t) - x_1(t)) = f_{k2}(\dot{x}_2 - v_{dr}), \end{aligned} \tag{7}$$

where m_i is the mass of the block, $a_i = \mathrm{d}^2 x_i / \mathrm{d}t^2$ its acceleration and $f_{ki}(\dot{x}_i - v_{dr})$ the kinetic friction force, usually a function of the velocity of the block relative to the belt. In general, the two blocks will not start slipping simultaneously and there will be intervals of time in which the motion of one block is described by equation (5) and the motion of the other by equation (7). For that reason the phase space dimension of the system may be 2 if both blocks are riding on the belt, 3 when one block is slipping and the second block is sticking, 4 when both blocks are slipping.

For a realistic expression of the kinetic friction force, if it is assumed that the driving velocity is small [9], then any transient motion characterized by a global stick phase will be attracted by a steady state motion with an infinite sequence of alternating slip phases and *global stick phases*. A global stick phase is a phase of motion in which both blocks are simultaneously sticking on the belt, whereas a slip phase is defined by the slipping of at least one block. In the space of the displacement variables it is possible to locate a region where the global stick phases have to lie: this is the region where all inequalities (6) hold simultaneously and will be called the *global stick phase locus*.

It is usually preferable to work with a dimensionless form of the above system given by the following equations, obtained for the case $m_1 = m_2 = m$, $k_1 = k_2 = k$:

$$\text{Stick phase} \quad X_i(\tau) = X_i(\tau_0) + V_{dr}(\tau - \tau_0), \quad i = 1, 2. \tag{5a}$$

$$\text{Global Stick phase locus} \quad \begin{aligned} -1 < X_1 + \alpha(X_1 - X_2) < 1, \\ -\beta < X_2 + \alpha(X_2 - X_1) < \beta. \end{aligned} \tag{6a}$$

$$\text{Slip phases} \quad \begin{aligned} \ddot{X}_1(\tau) + X_1(\tau) + \alpha(X_1(\tau) - X_2(\tau)) = F_{k1}(\dot{X}_1 - V_{dr}), \\ \ddot{X}_2(\tau) + X_2(\tau) + \alpha(X_2(\tau) - X_1(\tau)) = F_{k2}(\dot{X}_2 - V_{dr}), \end{aligned} \tag{7a}$$

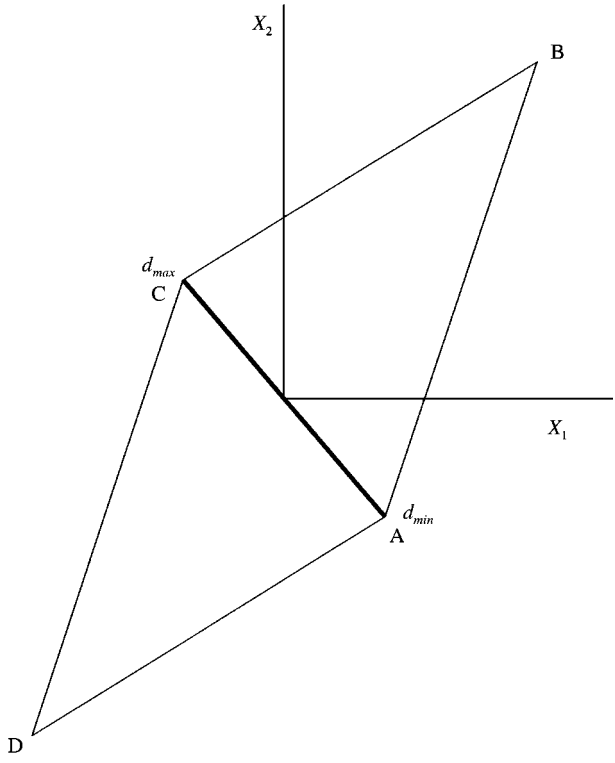

Figure 2. Global stick phase locus in the displacement space. The interval AC is the field of definition of the map defined by equation (12).

where $\beta = f_{s2}/f_{s1}$, $\alpha = k_{12}/k$, $X_i = kx_i/f_{s1}$, $\tau = \sqrt{k/m}t$, $V_{dr} = v_{dr}\sqrt{km}/f_{s1}$; note that τ is a dimensionless time and that $\mathrm{d}/\mathrm{d}t = \sqrt{k/m}\ (\mathrm{d}/\mathrm{d}\tau)$. Figure 2 shows the typical shape of a global stick phase locus.

The kinetic friction force may assume different forms, the most common of which is the Coulomb friction that, in dimensionless terms, is given by the following expression:

$$F_k(\dot{X} - V_{dr}) = \begin{cases} \mu_k & \text{if } V_{dr} > \dot{X}, \\ -\mu_k & \text{if } V_{dr} < \dot{X}, \end{cases} \tag{8}$$

where $0 < \mu_k < 1$ is a constant and therefore the kinetic friction is a constant force opposite to the relative motion between block and belt, smaller in magnitude than the maximum static friction force F_s ($F_s = 1$ in dimensionless terms). Note that for the system under investigation $\mu_{k2} = \beta\mu_{k1}$.

Another commonly used form of kinetic friction [7] is given in terms of three parameters:

$$F_k(\dot{X} - V_{dr}) = \begin{cases} \dfrac{1-\delta}{1-\gamma(\dot{X} - V_{dr})} + \delta + \eta(\dot{X} - V_{dr})^2 & \text{if } V_{dr} > \dot{X}, \\ -\dfrac{1-\delta}{1+\gamma(\dot{X} - V_{dr})} - \delta - \eta(\dot{X} - V_{dr})^2 & \text{if } V_{dr} > \dot{X}, \end{cases} \tag{9}$$

where γ is taken to be positive because the dynamic friction force is usually decreasing for small values of the relative velocity, η is positive because the dynamic friction force is usually assumed to be increasing for large values of the relative velocity, and finally δ may vary between 0 and 1 to avoid unrealistic changes of sign in the friction force. This second form of kinetic friction assumes the value 1 for zero relative velocity and therefore the friction force is continuous in the stick–slip transition, whereas the slip–stick transition is in general characterized by a finite jump in the friction force. With the Coulomb friction both transitions are discontinuous for the friction force. Figure 3 shows different forms of the friction characteristic (9). Note that in the system under investigation the kinetic friction force is defined according to the following relationship:

$$F_{k1} = F_k(\dot{X}_1 - V_{dr}),$$
$$F_{k2} = \beta F_k(\dot{X}_2 - V_{dr}). \tag{10}$$

It may be recalled how the two-block stick–slip system may generate a one-dimensional map [9]. During a global stick phase the relative displacements between the two blocks is fixed, and therefore the global stick phases of the system may be characterized by the constant value of a variable d:

$$d = X_2 - X_1. \tag{11}$$

The global stick phase will finish where one of the two blocks starts slipping, then the motion of the slipping block may trigger a new slipping phase for the other block also but eventually, if the driving velocity is small [9], both blocks will reach a configuration in which they ride simultaneously on the belt. The new global stick phase, in general, will be characterized by a value of the relative displacement d different from the one assumed during the previous global stick phase. In this way a motion of the system generates an infinite sequence of values of the variables $d = d_1, d_2, \ldots, d_m, \ldots$, which can be interpreted as a map expressing d_{k+1} as a function of d_k:

$$d_{k+1} = f(d_k). \tag{12}$$

Map (12) was first introduced in the seismological field [23] and for that reason it is called the *event-map*, since each iteration corresponds to a seismic event (earthquake) of the stick–slip model. In a periodic motion an integer j exists such that $d_{j+1} = d_1$; in this case the map is also periodic, of period j, whereas if a motion is not periodic it will generate a non-periodic map. The map is defined in the field obtained by projecting the *global stick phase locus* on the space of the variable d.

The boundary of the quadrilateral global stick phase locus (Figure 2) contains the points A and C corresponding to the two limit values d_{min}, d_{max} of the definition field of the map.

The mechanical system of Figure 1 is numerically integrated in continuous time with the algorithms described in reference [8]. The successive iterations of map (12) are then computed, according to equation (11), since the knowledge of the map makes the understanding of the dynamics of the mechanical system much simpler.

It is important to stress the fact that the 1-D map is well defined if the driving velocity is "small". In such a case any motion starting as a global stick phase will be attracted by a steady state motion characterized by global stick phases, as is clear in the examples shown in this paper. Even in the case of small driving velocity and, more probably with the Coulomb friction, steady state motions with no global stick phase can exist. The present

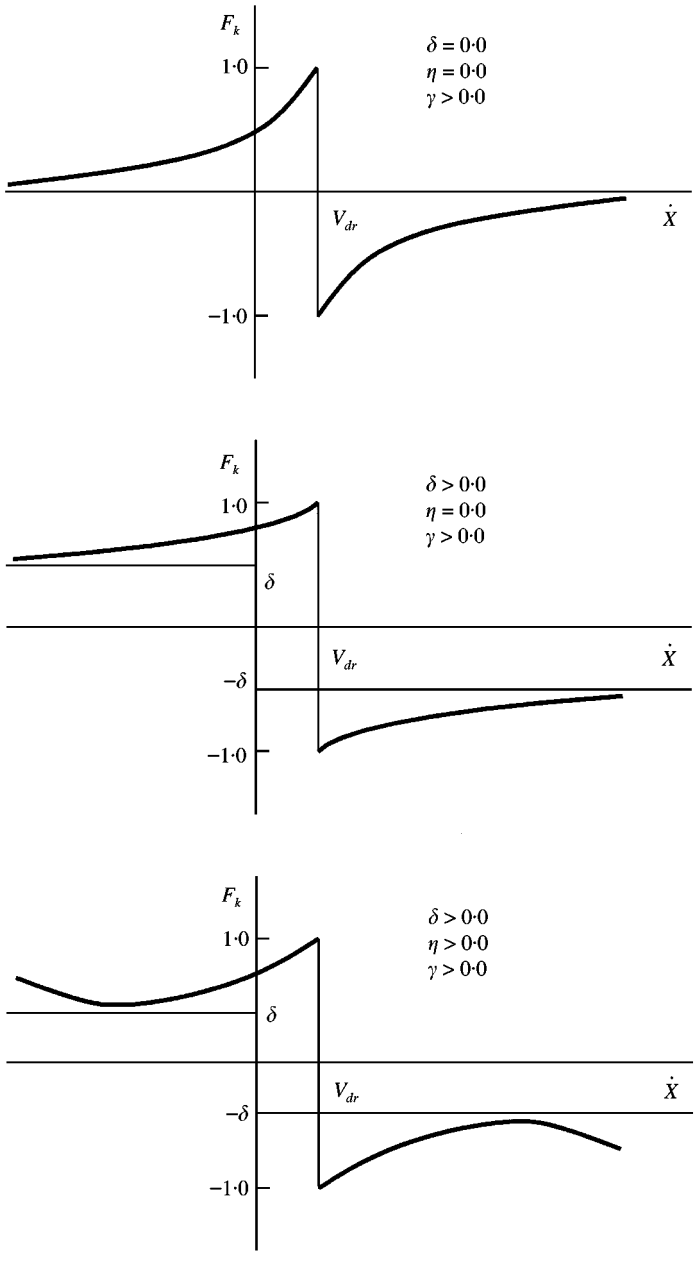

Figure 3. Different shapes of the friction characteristic (9) for different values of the constitutive parameters.

analysis, based on the use of the 1-D event map, does not consider steady state motions with no global stick phase.

4. DESCRIPTION OF THE BIFURCATIONS

Figure 4(a) shows the evolution of several steady state motions of the system with the Coulomb friction characterized by the following parameters: $\alpha = 1{\cdot}2$, $\beta = 1{\cdot}3$, $\mu_k = 0{\cdot}22$, in

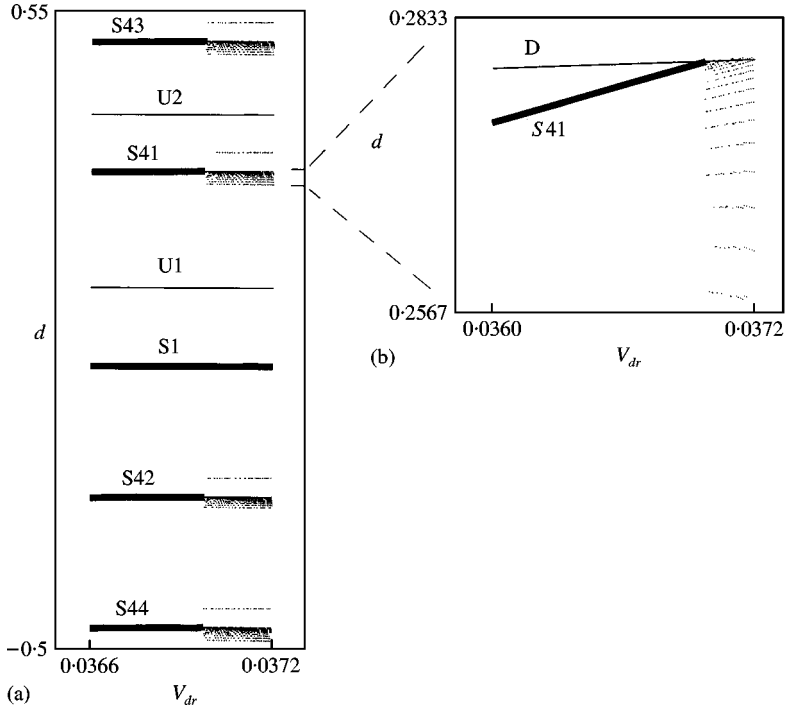

Figure 4. (a) Evolution of several steady state motions of the Coulomb system as the parameter V_{dr} is varied in the range $0{\cdot}0366 < V_{dr} < 0{\cdot}0372$. Thick lines represent periodic attractors, thin lines represent periodic unstable orbits, and points represent non-periodic attractors. (b) Enlarged view of a portion of figure (a). D represents a discontinuity line.

the range $0{\cdot}0366 < V_{dr} < 0{\cdot}0372$. For this $V_{dr} = 0{\cdot}0366$ at least two attractors exist, a period-1 motion S1 and a period-4 motion S4. Moreover, the period-1 unstable motions U1 and U2 are also present. For $V_{dr} \approx 0{\cdot}03698$ the dynamics of period-4 stable motion experiences a sudden transition from a period-4 motion to a non-periodic motion. In Figure 4(b) an enlarged view of the branch S41 of the attractor S4 is shown together with a line of discontinuity of the 1-D map previously defined. The figure gives evidence that the stable orbit S4 becomes a non-periodic orbit at a collision with the line of discontinuity of the map. Figure 5 shows the 1-D event map for $V_{dr} = 0{\cdot}0366$. The stable period-4 motion gives rise to a period-4 map and one of the four periodic points (point 1 in Figure 5) is close to a discontinuity point of the map. As V_{dr} is increased the sudden transition to a non-periodic motion corresponds to the collision between the periodic point 1 and the discontinuity of the map. Figure 6 shows the 1-D map and its new attractor for $V_{dr} = 0{\cdot}037$.

Examination of the phase portrait of block 2 reveals that such a transition is linked to a grazing orbit. Figure 7 illustrates the evolution of the steady state motion of the second block as V_{dr} varies between 0·0366 and 0·037. For $V_{dr} = 0{\cdot}0366$ (Figure 7(a)) a lobe of the periodic orbit is close to a tangency with the line $V_2 = V_{dr}$, as V_{dr} is increased the lobe of the orbit approaches the stick interval and it touches it for $V_{dr} \approx 0{\cdot}03698$. For $V_{dr} = 0{\cdot}0370$ (Figure 7(b)) the steady state motion no longer appears periodic and keeps intersecting the stick interval in proximity to the point $X_2 = 0$.

This bifurcation seems to be due to the peculiar nature of the definition of the Coulomb friction in the common case of a kinetic friction coefficient smaller than the static coefficient, i.e., $\mu_k < 1$ in dimensionless notation. The equations of motion (7a) can be rewritten as

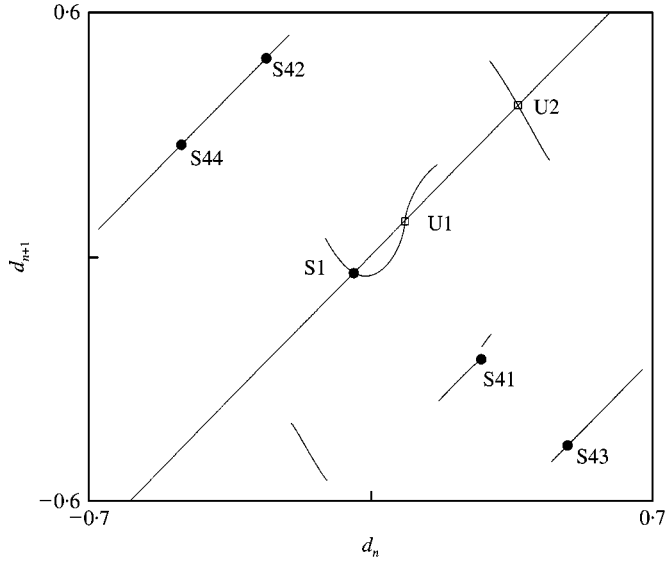

Figure 5. Event map of the Coulomb system for $V_{dr} = 0{\cdot}0366$. Bold points indicate the periodic attractors of Figure 4, squares indicate period-1 unstable orbits.

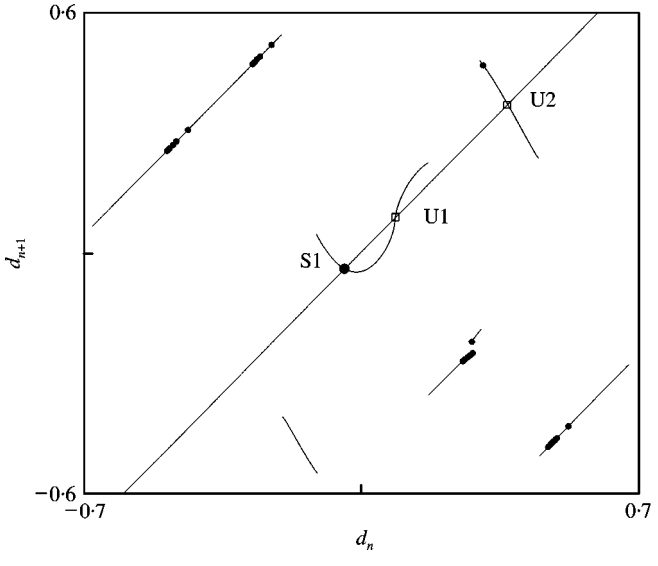

Figure 6. Event map of the Coulomb system for $V_{dr} = 0{\cdot}0370$. Bold points indicate the non-periodic attractor of Figure 4.

a system of first order ordinary differential equations. In this case, the motion equation of block 2 becomes:

$$\dot{X}_2 = Y_2,$$
$$\dot{Y}_2 = -X_2(\tau) - \alpha(X_2(\tau) - X_1(\tau)) + \beta\mu_k. \tag{13}$$

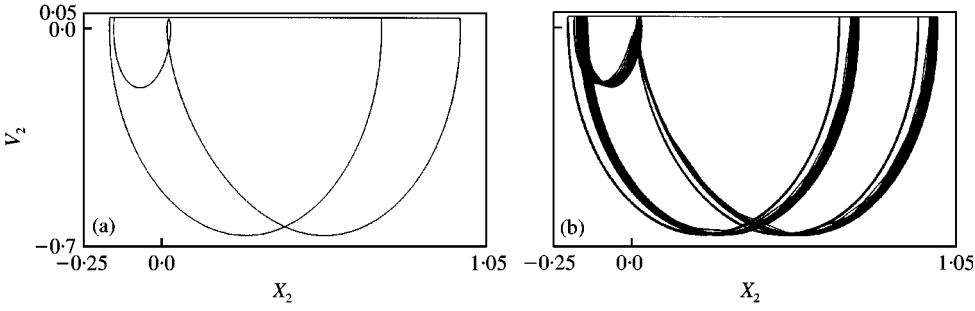

Figure 7. Phase plots of the steady state motions of block 2 for (a) $V_{dr} = 0{\cdot}0366$, and (b) $V_{dr} = 0{\cdot}0370$.

Equation (13b) provides the condition for having a point of the trajectory with horizontal tangent:

$$\dot{Y}_2 = -X_2(\tau) - \alpha(X_2(\tau) - X_1(\tau)) + \beta\mu_k = 0. \tag{14}$$

If such a condition is verified when $Y_2 = V_{dr}$ then the trajectory is tangent to the stick interval. This is the case shown in Figure 7. Once the trajectory has reached the stick interval then static friction conditions apply and, since equation (14) is verified, the tangent point becomes a sticking point for block 2. Block 2 will leave the sticking interval when the right end of the sticking interval is reached, i.e., when the following equation holds true:

$$X_2(\tau) + \alpha(X_2(\tau) - X_1(\tau)) = \beta. \tag{15}$$

Therefore, the discontinuous definition of the laws of motion justifies the discontinuous bifurcation shown in Figure 4. Such a type of discontinuous bifurcation would be avoided if the kinetic friction coefficient were equal to the static friction coefficient, i.e., if $\mu_k = 1$. Nonetheless, in such a case the experimental evidence of a smaller kinetic friction force would be lost.

Figure 8 shows the fourth iterated map for $V_{dr} = 0{\cdot}0366$ (Figure 8(a)) and two enlarged portions of the same map, again for $V_{dr} = 0{\cdot}0366$ (Figure 8(b)), and for $V_{dr} = 0{\cdot}0372$ (Figure 8(c)). In this figure, the bifurcation appears to be similar to the bifurcation described in reference [14], where a stable periodic orbit collides with an infinitely unstable periodic orbit at a discontinuous fold bifurcation in the dynamics of a 1-d.o.f. stick–slip system. In the case of reference [14] the infinitely unstable orbit is the separatrix between the basins of attraction of two coexisting attractors and it is also possible to identify such an orbit by integrating backwards in time an orbit tangent to the sticking interval. The system under investigation in the present paper is more complex but it can be said that the existence of a possible separatrix orbit between basins of different attractors, is not apparent since both branches of the discontinuous map belong to the same basin of attraction, as shown in Figure 9. The behaviour of the system suggests the idea that an infinitely unstable orbit, U4, may exist which divides the orbits that are attracted by the same attractor S4. Figure 10 shows that orbits on different sides of the diagonal at the discontinuity point are attracted to S4 in different ways. A period-4 infinitely unstable orbit, characterized by the approximated values $(-0{\cdot}466,\ -0{\cdot}254,\ +0{\cdot}279,\ +0{\cdot}492)$, exists in the basin of attraction of S4. For $V_{dr} \approx 0{\cdot}03698$, S4 and U4 collide but such a collision do not cause the merger of two basins of attraction as in reference [14]. In the present case S4 is substituted by a non-periodic attractor that has its same basin of attraction. The slope of the map at the intersection

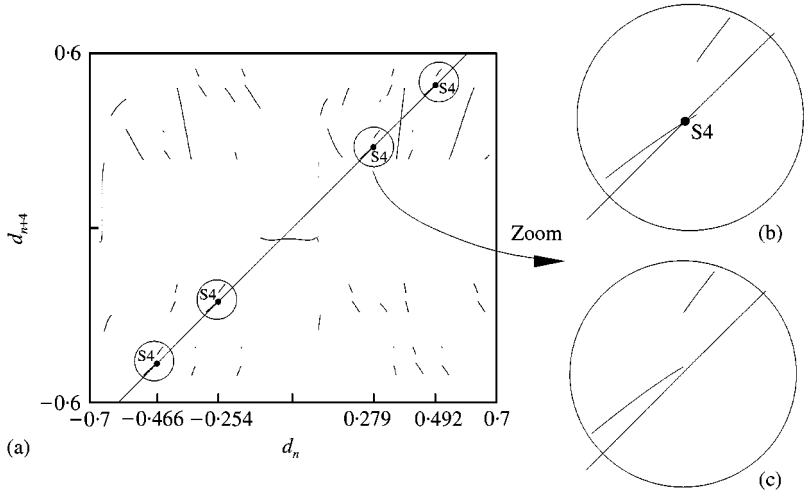

Figure 8. Fourth iterated maps (a) for $V_{dr} = 0{\cdot}0366$, circles indicate the period-4 stable orbit, (b) enlarged view for $V_{dr} = 0{\cdot}0366$, (c) enlarged view for $V_{dr} = 0{\cdot}0372$.

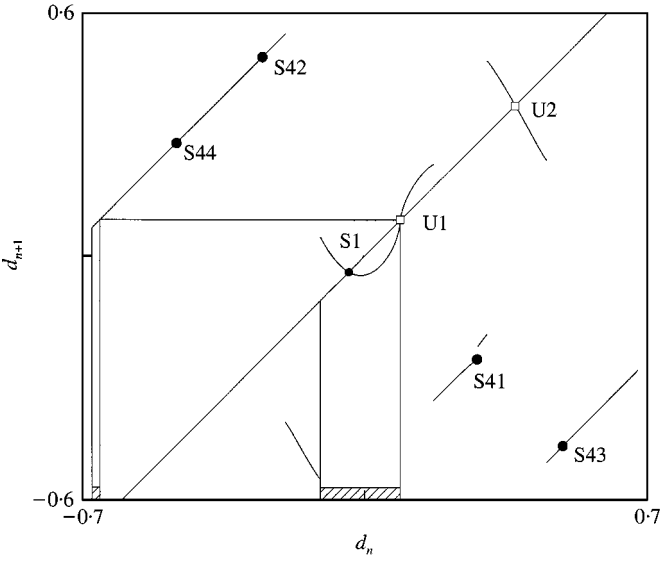

Figure 9. Basins of attraction of the 1-D map for $V_{dr} = 0{\cdot}0366$: the hatched region is the basin of S1, the remaining part of the interval of definition of the 1-D map is the basin of attraction of S4.

points of the periodic solutions is equal to Floquet multiplier [14]. From Figure 10 it is therefore clear that at the bifurcation point a Floquet multiplier jumps across the unit circle from a positive value close to one to infinity.

The second example of non-smooth bifurcation is taken from the dynamics of the stick–slip system with kinetic friction given by equation (9). The parameters of the system are: $\beta = 1{\cdot}301$, $V_{dr} = 0{\cdot}295$, $\delta = 0$, $\eta = 0$, $\gamma = 3$, in the range $1{\cdot}20800 < \alpha < 1{\cdot}21865$. Several attractors may exist for the above-mentioned set of parameters but the present analysis is only focused on the range of values $0{\cdot}379 < d < 0{\cdot}390$, where a rich variety of smooth and non-smooth bifurcations can explain the sudden variations in the dynamics of the system.

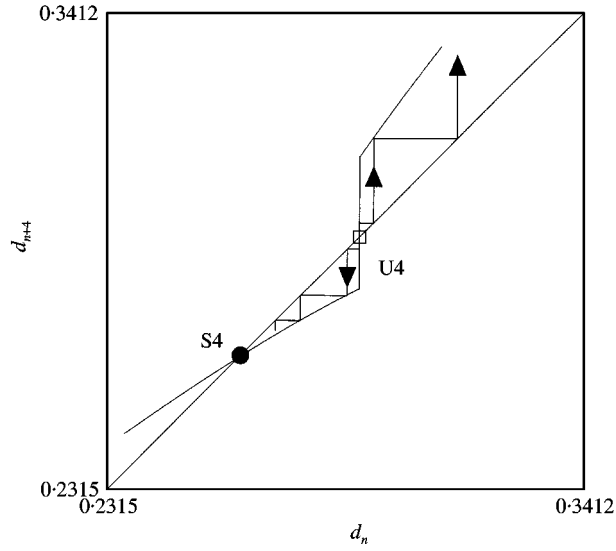

Figure 10. Portion of the fourth iterated map for $V_{dr} = 0{\cdot}0366$. Orbits starting on different sides of the discontinuity are all attracted by S4, but their initial transients are significantly different. U4 is the infinitely unstable period-4 orbit.

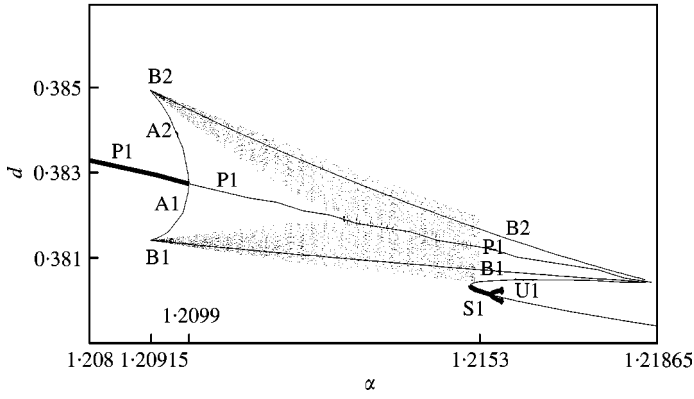

Figure 11. Bifurcation diagram of the two-block system with friction law (9). Thick lines indicate periodic attractors, thin lines periodic unstable motions, dots non-periodic attractors.

Figure 11 illustrates some of the steady state motions of the system; the bifurcations affecting them are described in the present section. The examination of the previously defined 1-D map allows a clear description of the evolution of the attractors. If the period-1 attractor, called P1 in Figure 11, is followed for increasing values of the parameter α it is possible to notice that it changes stability for $\alpha \approx 1{\cdot}2099$ and then disappears at $\alpha \approx 1{\cdot}21865$. In a smaller interval of the α variable also a non-periodic attractor suddenly appears at $\alpha \approx 1{\cdot}20915$ and then disappears at $\alpha \approx 1{\cdot}2153$. Figure 12(a) shows the first iterated map, $d_{n+1} = f(d_n)$, and Figure 12(b) the second iterated map, $d_{n+2} = g(d_n)$, for $\alpha = 1{\cdot}208$. The stable period-1 fixed point is clearly shown. Note that a cusp is present in the first iterated map and two cusps are present in the second iterated map. The non-smooth bifurcations described below are due to the intersection of the cusps with the lines $d_{n+1} = d_n$ or $d_{n+2} = d_n$. For $\alpha \approx 1{\cdot}20915$ the two cusps of the second iterated map, g, intersect the line

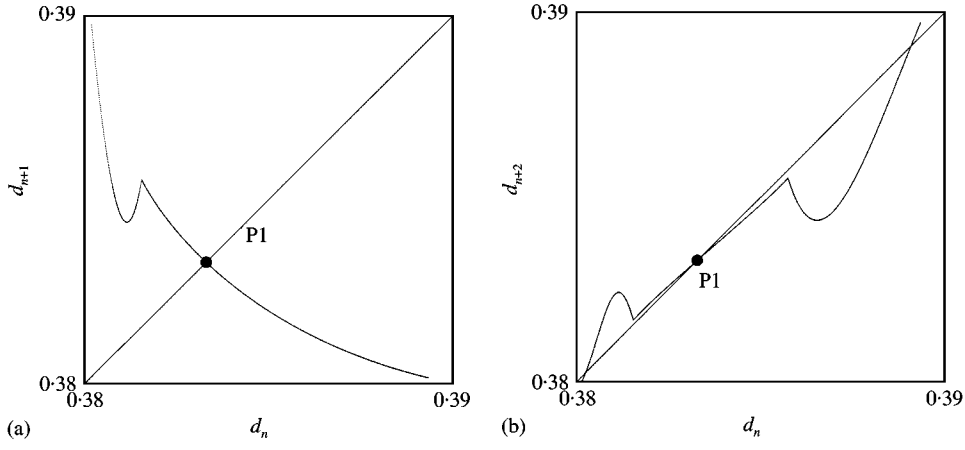

Figure 12. First iterated map (a) and second iterated map (b) for $\alpha = 1{\cdot}208$.

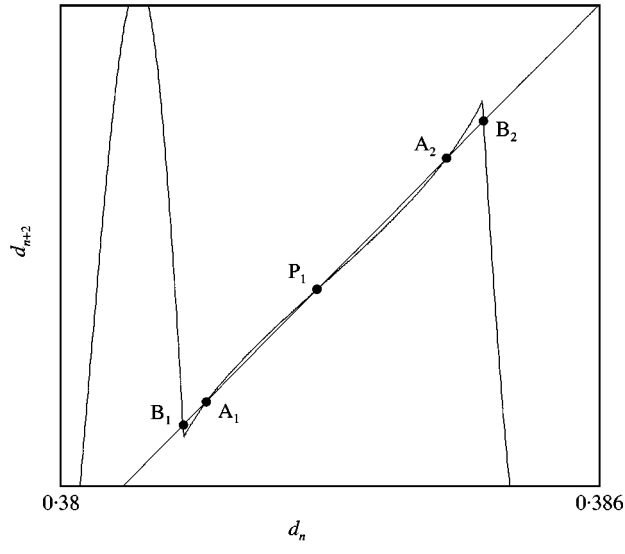

Figure 13. Second iterated map for $\alpha = 1{\cdot}20915$. The vertical distance between the map and the line $d_{n+2} = d_n$ is magnified.

$d_{n+2} = d_n$. Figure 13 shows the g map just after the bifurcation point. Note that in Figure 13 the distance between the map and the line $d_{n+2} = d_n$ is magnified to make the diagram more clear. The map would be almost indistinguishable from the line without such a magnification. At least two period-2 unstable orbits are born at this bifurcation; they are labelled A1–A2 and B1–B2 in Figures 13 and 11. Numerical calculations suggest that also a non-periodic attractor is created at the same point. As α is increased, the A1–A2 period-2 orbit approaches the attractor P1, as shown in Figure 11. At the value $\alpha \approx 1{\cdot}2099$ P1 and A1–A2 collide in an apparently smooth subcritical flip bifurcation following which the period-2 unstable orbit disappears and the period-1 attractor becomes unstable, as shown in Figure 11. Moreover, as α is increased, the two bands of the chaotic attractor become wider while the distance between them reduces (see Figure 11). The unstable orbit B1–B2 is embedded in the chaotic attractor, as shown in Figure 11. Figure 14 shows the first and the

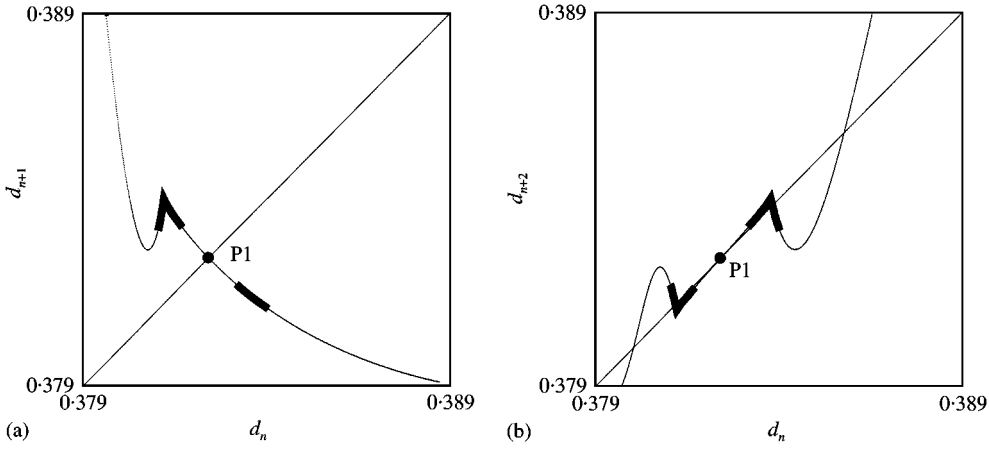

Figure 14. First iterated map (a) and second iterated map (b) for $\alpha = 1{\cdot}211$.

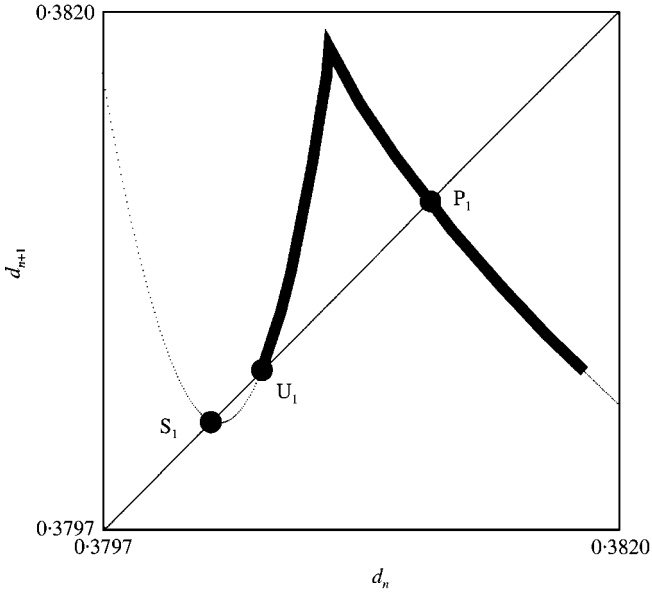

Figure 15. Collision between the non-periodic attractor and its basin boundaries for $\alpha \approx 1{\cdot}2153$. Thick lines indicate the chaotic attractor, thin dots transient motions, thick dots steady state motions.

second iterated maps for $\alpha = 1{\cdot}211$: the chaotic attractor is indicated by thick lines while transient points of the map are represented by thin lines. Note that the first iterated map, f, presents a lobe with horizontal tangent that approaches the line $d_{n+1} = d_n$ as α is increased. For $\alpha \approx 1{\cdot}2151$ an apparently smooth fold bifurcation occurs in f. Two period-1 orbits are born, S1 stable and U1 unstable. U1 will play a crucial role in the disappearance of the chaotic attractor. In fact the chaotic attractor collides with one of the boundaries of its basin, represented by U1, for $\alpha \approx 1{\cdot}2153$ (Figure 15). The collision between a chaotic attractor and its basin boundaries is a well-known phenomenon that was also observed in stick–slip systems [24]. After the collision the chaotic attractor disappears and the transient trajectories, which for smaller values of α were attracted by it, are now attracted by S1. The

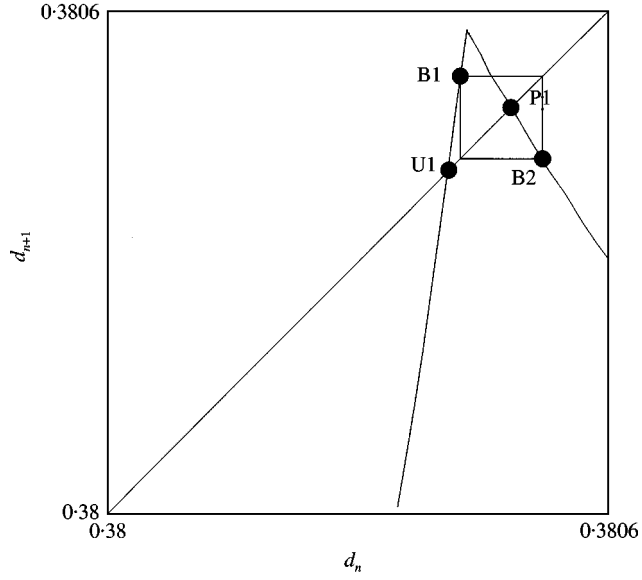

Figure 16. First iterated map for $\alpha = 1{\cdot}2182$.

period-1 motion S1 then undergoes an apparently smooth period-doubling cascade, which will not be described below. The first branches of the period-doubling cascade are shown in Figure 11, but the other branches are not shown for reasons of clarity.

Finally, the unstable motions P1, U1 and B1–B2 disappear simultaneously at a further discontinuous bifurcation close to $\alpha \approx 1{\cdot}21865$ when the cusp of the first iterated map intersects the line $d_{n+1} = d_n$. Figure 16 shows the first iterated map for a value of α slightly smaller than the bifurcation value. At the bifurcation point the three unstable motions coincide.

The two bifurcations of Figures 13 and 16 appear very similar. For $\alpha \approx 1{\cdot}20915$ and for increasing values of α, or for $\alpha \approx 1{\cdot}21865$ and decreasing values of α, a cusp intersects the line $d_{n+1} = d_n$. In both cases, the slope of the map is set-valued with a finite difference between the values of the slopes meeting at the bifurcation point. Nonetheless, it is clear from the previous description that in the first case a chaotic attractor is created together with an unknown number of unstable orbits, whereas in the second case only unstable orbits are generated. The different outcome of the two bifurcations cannot be inferred only from the "local shape" of the map, i.e., it is not only due to the different slopes of the two branches of the map meeting at the cusp point. It also depends on the shape of the map in zones away from the cusp. In the case of Figure 13, the map is folded in such a way that orbits leaving the cusp zone are brought back to it, and in this manner a chaotic attractor is generated. In the case of Figure 16 no folding-back process is present so that only unstable orbits are generated at the non-smooth bifurcation.

Also, the discontinuous bifurcations of the present example seem to be linked to trajectories tangent to the sticking interval. Figure 17 shows two transient trajectories for $\alpha = 1{\cdot}208$. Initial conditions are chosen in such a way that the motion of Figure 17(a) has an initial value of d slightly smaller than the value corresponding to the cusp of the map, whereas motion in Figure 17(b) is characterized by a slightly larger initial value of d. The numerical integration in interrupted as soon as the trajectory has reached a sticking condition. The figure suggests the idea that the cusps of the maps correspond to orbits tangent to the sticking interval.

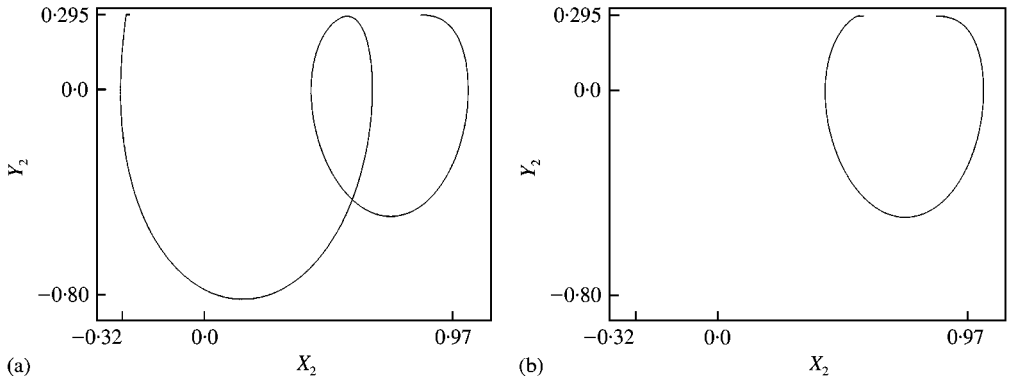

Figure 17. Transient trajectories for $\alpha = 1{\cdot}208$. Initial conditions (a) $d = 0{\cdot}3812$; (b) $d = 0{\cdot}3818$. The "cusp value" of d is approximately 0·3815.

In the case of friction law in equation (9) the points with horizontal tangent are characterized by the condition:

$$\dot{Y}_2 = -X_2(\tau) - \alpha(X_2(\tau) - X_1(\tau)) + \beta F_k(Y_2 - V_{dr}) = 0. \tag{16}$$

Therefore, the only points where a trajectory can be tangent to the sticking interval are the endpoints of the interval itself: at these points the trajectory reaches the sticking interval and, at the same time, leaves it since condition (16) is verified. Similar bifurcations have been also found in references [14, 25]. However, in reference [14] the full Poincaré map is a mapping from $\mathbb{R}^2$ to $\mathbb{R}^2$ which cannot be easily visualized, whereas the event map described in the present paper fully describes the dynamics of the *global stick phase* steady state motions, as specified at the end of section 3.

5. CONCLUSIONS

The paper presents two non-smooth bifurcations affecting stick–slip systems. The first bifurcation affects a system with the Coulomb friction and can be described as a collision between an attractor and an infinitely unstable orbit of a suitably defined 1-D map. The definition of a kinetic friction coefficient smaller than the static one seems to be the main cause of the discontinuous bifurcation. The second bifurcation affects a system with a continuous friction law and is due to the intersection of certain cusps of the same 1-D map with the line $d_{n+1} = d_n$.

ACKNOWLEDGMENT

Very constructive comments by an anonymous reviewer are gratefully acknowledged.

REFERENCES

1. H. TRUE 1999 *Vehicle System Dynamics* **31**, 393–421. On the theory of nonlinear dynamics and its applications in vehicle systems dynamics.
2. S. H. DOOLE and S. J. HOGAN 1996 *Dynamics and Stability of Systems* **11**, 19–47. A piecewise linear suspension bridge model: nonlinear dynamics and orbit continuation.

3. S. J. HOGAN 2000 *Chaos, Solitons and Fractals* **11**, 495–506. Damping in rigid block dynamics contained between side-walls.
4. S. R. BISHOP 1994 *Philosophical Transactions of the Royal Society of London A* **347**, 347–351. Impact oscillators.
5. C. J. BUDD and A. G. LEE 1996 *Philosophical Transactions of the Royal Society of London A* **452**, 2719–2750. Double impact orbits of periodically forced impact oscillators.
6. M. WIERCIGROCH, R. D. NEILSON and M. A. PLAYER 1999 *Physics Letters A* **259**, 91–96. Material removal rate prediction for ultrasonic drilling of hard materials using an impact oscillator approach.
7. K. POPP and P. STELTER 1990 *Philosophical Transactions of the Royal Society of London A* **332**, 89–105. Stick–slip vibrations and chaos.
8. U. GALVANETTO and S. R. BISHOP 1998 *Computer Methods in Applied Mechanics and Engineering* **163**, 373–382. Computational techniques for non-linear dynamics in multiple friction oscillators.
9. U. GALVANETTO 1999 *Computer Methods in Applied Mechanics and Engineering* **178**, 291–306. Nonlinear dynamics of multiple friction oscillators.
10. M. WIERCIGROCH, V. W. T. SIN and Z. F. K. LIEW 1999 *Proceedings of the Institute of Mechanical Engineers Part C—Journal of Mechanical Engineering Science* **213**, 527–533. Non-reversible dry friction oscillator: design and measurements.
11. M. KUNZE and T. KUPPER 1997 *ZAMP* **48**, 87–101. Qualitative bifurcation analysis of a non-smooth friction-oscillator model.
12. B. L. VAN DE VRANDE, D. H. VAN CAMPEN and A. DE KRAKER 1999 *Nonlinear Dynamics* **19**, 157–169. An approximate analysis of dry-friction-induced stick–slip vibrations by a smoothing procedure.
13. M. DI BERNARDO, C. J. BUDD and A. CHAMPNEYS 1998 *Nonlinearity* **11**, 859–890. Grazing, skipping and sliding: analysis of the non-smooth dynamics of the DC/DC buck converter.
14. R. I. LEINE, D. H. VAN CAMPEN and B. L. VAN DE VRANDE 2000 *Nonlinear Dynamics* **23**, 105–164. Bifurcations in nonlinear discontinuous systems.
15. A. FILIPPOV 1964 *American Mathematical Society Translations, Series* 2 **42**, 199–231. Differential equations with discontinuous right-hand side.
16. J. GUCKENHEIMER and P. HOLMES 1997 *Nonlinear Oscillations, Dynamical Systems, and Bifurcations of Vector Fields*. Berlin: Springer-Verlag.
17. N. HINRICHS, M. OESTREICH and K. POPP 1997 *Chaos Solitons and Fractals* **8**, 535–558. Dynamics of oscillators with impact and friction.
18. A. B. NORDMARK 1991 *Journal of Sound and Vibration* **145**, 279–297. Non-periodic motion caused by grazing incidence in an impact oscillator.
19. H. DANKOWICZ and A. B. NORDMARK 2000 *Physica D* **136**, 280–302. On the origin and bifurcations of stick–slip oscillations.
20. M. DI BERNARDO, M. I. FEIGIN, S. J. HOGAN and M. E. HOMER 1999 *Chaos, Solitons and Fractals* **10**, 1881–1908. Local analysis of C-bifurcations in n-dimensional piecewise-smooth dynamical systems.
21. H. E. NUSSE and J. A. YORKE 1992 *Physica D* **57**, 39–57. Border collision bifurcations including period two to period three for piecewise smooth systems.
22. S. BANERJEE, R. PRYIA and C. GREBOGI 2000 *IEEE Transactions on Circuits and Systems-I: Fundamental Theory and Applications* **47**, 633–643. Bifurcations in two-dimensional piecewise smooth maps—theory and applications in switching circuits.
23. J. NUSSBAUM and A. RUINA 1987 *Pure and Applied Geophysics* **125**, 629–656. A two degree-of-freedom earthquake model with static dynamic friction.
24. U. GALVANETTO 1997 *Journal of Sound and Vibration* **204**, 690–695. Bifurcations and chaos in a 4-dimensional stick–slip system.
25. Y. YOSHITAKE and A. SUEOKA 2000 in *Applied Nonlinear Dynamics and Chaos in Mechanical Systems* (M. Wiercigroch and A. de Kraker, editors). Singapore: World Scientific. Forced self-excited vibration accompanied by dry friction.